

Some phase transformations in steels

H. K. D. H. Bhadeshia

Many essential properties of iron alloys depend on the atomic mechanism of phase change. Following a description of the mechanisms established for solid state transformations in steels, a unique measure of the mechanism is proposed, one which can easily be accessed experimentally. The application of the mechanism to the design of novel steels is illustrated in the context of martensite and bainite. This is followed by an introduction to a new and quite general kinetic theory based on the Avrami approach. The application of the theory to creep resistant and structural steels is illustrated with example calculations. MST/4155

The author is in the Department of Materials Science and Metallurgy, University of Cambridge, Pembroke Street, Cambridge CB2 3QZ, UK. This paper formed part of the 'Advances in physical metallurgy' sessions of Materials Congress '98 organised by The Institute of Materials and held at Cirencester on 6–8 April 1998.

© 1999 IoM Communications Ltd.

Introduction

About 70% of all the steel compositions that are currently used have been developed within the last 10 years. Novel iron alloys are being conceived, manufactured, and marketed with a regularity which has confounded many prophecies. Phase transformation theory has contributed to the successful development of steels. This overview will begin therefore with a discussion of the atomic mechanism by which phase changes are achieved in steels.

Mechanisms of transformation

The atomic arrangement in a crystal can be altered (Fig. 1) either by breaking all the bonds and rearranging the atoms into an alternative pattern (*reconstructive* transformation), or by homogeneously deforming the original pattern into a new crystal structure (*displacive* transformation).

In the displacive mechanism the change in crystal structure also alters the macroscopic shape of the sample when the latter is not constrained. The shape deformation during constrained transformation is accommodated by a combination of elastic and plastic strains in the surrounding matrix. The product phase grows in the form of thin plates to minimise the strains. The atoms are displaced into their new positions in a coordinated motion. Displacive transformations can therefore occur at temperatures where diffusion is inconceivable within the time scale of the experiment. Some solutes may be forced into the product phase, a phenomenon known as solute trapping. Both the trapping of atoms and the strains make displacive transformations less favourable from a thermodynamic point of view.

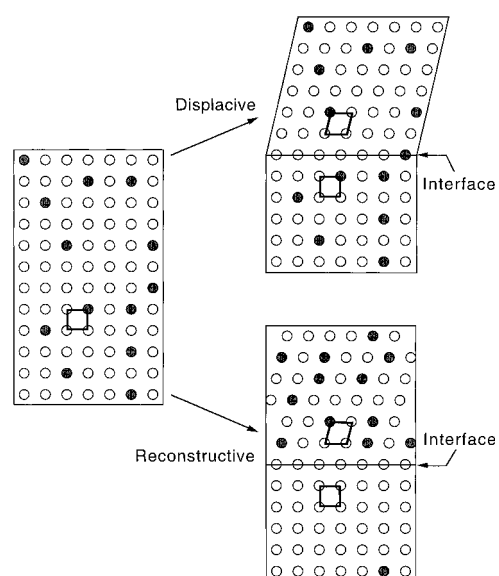
It is the diffusion of atoms that leads to the new crystal structure during a reconstructive transformation. The flow of matter is sufficient to avoid any shear components of the shape deformation, leaving only the effects of volume change. This diffusion is necessary even when transformation occurs in pure iron.¹ In alloys, the diffusion process may also lead to the redistribution of solutes between the phases in a manner consistent with a reduction in the overall free energy. Figure 2 is a summary of the main transformations that occur in steels.

Challenge

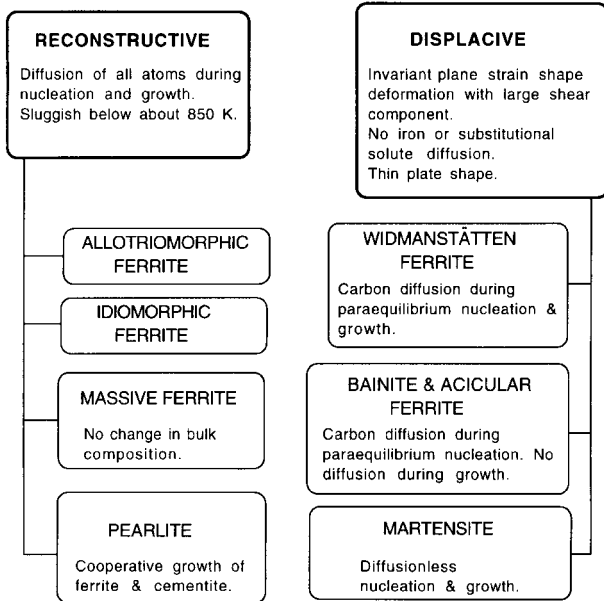
There has been much discussion about the mechanism of phase transformations in steels. It is, however, easy to

resolve the details necessary for the description of solid state transformations in steels.

Hexagonal close packed (hcp) ϵ -iron is stable only at pressures above 130 kbar at room temperature. Nevertheless, there are experiments where ϵ -iron has been observed at pressures as low as 80 kbar. These experiments were carried out using shock waves to generate the required pressure. The time scale is then so short that the mechanism is displacive with a glissile ϵ/α interface.² The defects introduced during shock deformation make it difficult for the transformation front to glide reversibly so there is a large *hysteresis*, as illustrated in Fig. 3. At ambient temperature, ϵ -iron forms in increasing quantities as the pressure is increased beyond 130 kbar. But when the pressure is subsequently reduced, the ϵ -iron does not revert to ferrite until 81 kbar, the specimen only becoming fully ferritic when the pressure becomes less than 45 kbar. Deviations like these are much smaller when the ϵ -iron transforms by a reconstructive mechanism. The defects in the austenite do not interfere with the uncoordinated transfer of atoms at the interface. On the contrary, they encourage a faster rate of transformation as the defects are eliminated by the passage of the interface in a process akin to recrystallisation.



1 Main mechanisms of transformation: parent crystal contains two kinds of atoms; figures on right represent partially transformed samples with parent and product unit cells outlined in bold; transformations are unconstrained in this illustration



2 Summary of essential characteristics of solid state transformations in steels

The retardation of a displacive transformation by dislocation debris is called *mechanical stabilisation*.⁴ It is argued here that mechanical stabilisation is a unique feature of displacive transformations:

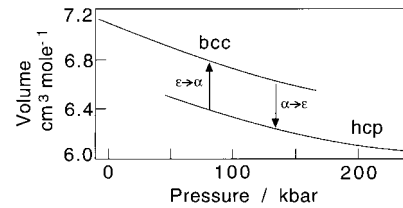
- (i) there is no mechanism by which plastic deformation can retard a reconstructive transformation: in fact, reconstructive transformations are always accelerated by defects in the austenite
- (ii) only displacive transformations can be mechanically stabilised; this is because they are associated with glissile interfaces whose motion becomes difficult in a matrix containing a forest of dislocations or other defects.

This forms the basis of a *rigorous* distinction between the two mechanisms of transformation, a distinction which has never been challenged either experimentally or with theoretical arguments. It has been proven that Widmanstätten ferrite, bainite, martensite, and mechanical twinning can all be retarded by the plastic deformation of austenite before transformation. On the other hand, allotriomorphic ferrite, pearlite, and recrystallisation reactions are always accelerated by such deformation. It will now be demonstrated how the theory of transformations can contribute to better alloys.

Crystallography of displacive transformation

It is important to understand the crystallography of displacive transformations since it influences many of the features of microstructure. The Bain strain **B** converts the structure of the parent phase into that of the product. When combined with an appropriate rigid body rotation, the net homogeneous lattice deformation **RB** is an invariant line strain (Fig. 4), giving good fit only along a single line common to the two crystals. However, the observed shape deformation indicates a larger degree of fit. The shape change is in fact an invariant plane strain (IPS) **P**₁, but this gives the wrong crystal structure. If, however, a second homogeneous shear **P**₂ is combined with **P**₁, then the correct structure is obtained but the wrong shape since

$$P_1 P_2 = RB \quad \dots \dots \dots (1)$$



3 Illustration of pressure hysteresis (overshooting of equilibrium transformation pressure of 130 kbar) of α⇌ε martensitic transformation.³ Vertical arrows indicate pressures at which α→ε and ε→α changes begin

These discrepancies are all resolved if the shape changing effect of **P**₂ is cancelled macroscopically by an inhomogeneous lattice invariant deformation, which may be slip or twinning as illustrated in Fig. 4.

The theory illustrated explains all the essential features of martensite or bainite crystallography.⁵⁻⁸ It is easy to predict the orientation relationship, by deducing the Bain strain and adding a rigid body rotation which makes the net lattice deformation an invariant line strain. The habit plane does not have rational indices because the amount of lattice invariant deformation needed to recover the correct macroscopic shape is not usually rational. The theory predicts a substructure in plates of martensite (either twins or slip steps), as is observed experimentally. The transformation produces a shape deformation that is macroscopically an invariant plane strain because this reduces the strain energy when compared with the case where the shape deformation might be an invariant line strain.

The mechanism of transformation outlined above is valid for martensite, bainite, and Widmanstätten ferrite, though there are subtle differences. It is not appropriate here to discuss these in detail, but some of the important characteristics are highlighted in Table 1. The relationship between mechanical properties and the mechanism of transformation will now be considered.

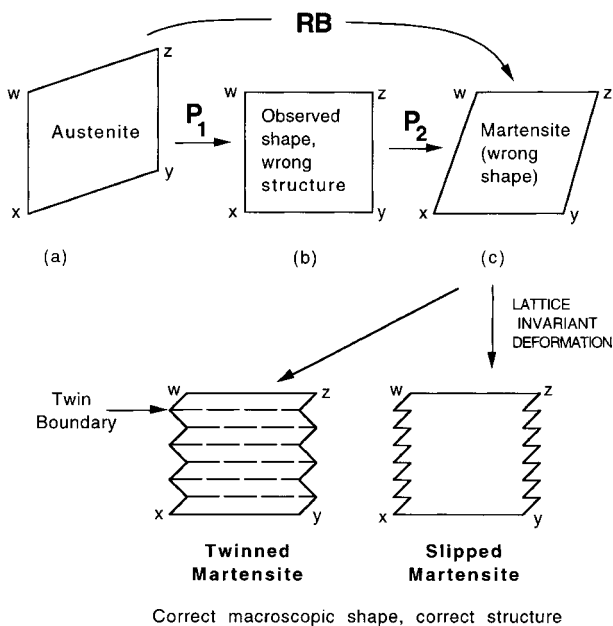
Quantitative fracture toughness

Much of the literature about toughness tends to focus on micromechanisms, test methodology, or procedures for using experimental data in design exercises. By contrast, there is very little work on the *prediction* of the energy absorbed during fracture. This difficulty is illustrated by some basic concepts of fracture mechanics. The critical value *K*_{1C} of the stress intensity which must be exceeded to induce rapid crack propagation is the product of two terms

$$K_{1C} = \text{stress} \times \text{distance}^{1/2} \quad \dots \dots \dots (2)$$

Table 1 Transformation characteristics for Widmanstätten ferrite α_w, bainite α_b, and martensite α' (Ref. 8)

	α'	α _b	α _w
Nucleation and growth reaction	✓	✓	✓
Plate shape	✓	✓	✓
Diffusionless nucleation	✓	x	x
Carbon diffusion during nucleation	x	✓	✓
Substitutional diffusion during nucleation	x	x	x
Confined to austenite grains	✓	✓	✓
Large shear	✓	✓	✓
Invariant plane strain shape deformation	✓	✓	✓
Diffusionless growth	✓	✓	x
Carbon diffusion during growth	x	x	✓
Substitutional diffusion during growth	x	x	x
Glissile interface	✓	✓	✓



4 Illustration of phenomenological theory of martensite crystallography⁷

where the stress is a fracture stress σ_F which can be measured independently using notched tensile specimens. It can be related to the microstructure via^{9,10}

$$\sigma_F \propto [E\gamma_p/\pi(1 - \nu^2)c]^{1/2} \dots \dots \dots (3)$$

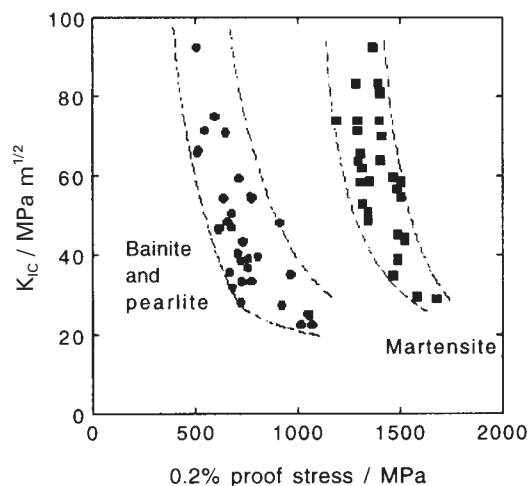
where E is the Young's modulus and ν is the Poisson's ratio. The term γ_p is the effective work done in creating a unit area of crack plane, estimated to be about 14 J m^{-2} for many iron base microstructures;¹¹ it is much larger than a surface energy (typically 1 J m^{-2}) because of the plastic zone which moves with the crack tip. This value of 14 J m^{-2} seems to apply to a wide variety of steel microstructures,¹¹ which is surprising given that they often have quite different deformation characteristics. In any event, there is no obvious way of relating γ_p to the details of the microstructure. By contrast, the dimension c is usually attributed to the size of a sharp crack created by the fracture of a brittle microstructural constituent such as a cementite particle or a non-metallic inclusion.

The other parameter in equation (2), distance^{1/2}, refers to a length ahead of the crack tip, within which the stress is large enough to cause the fracture of brittle crack initiators.

It is now appropriate to examine the observed fracture toughness behaviour for engineering steels with bainitic or martensitic microstructures. It is evident from Fig. 5 that bainitic steels are far more brittle than martensitic steels. Microscopic cleavage fracture stress σ_F for the bainitic steels is between 1100 and 2200 MPa, whereas that of martensite is about 3100–4000 MPa, approximately independent of temperature.¹² This can be explained if the distance c in equation (3) is equated to the cementite

Table 2 Cementite particle sizes in steel microstructures¹¹

Microstructure	Mean cementite size, nm	Coarsest particle, nm
Autotempered martensite	14	36
Tempered martensite	38	110
Severely tempered martensite	230	600
Upper bainite	220	1000
Mixed upper and lower bainite	230	720



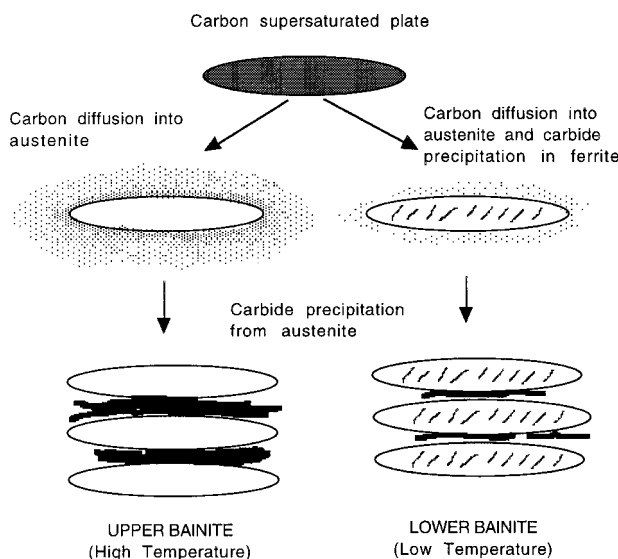
5 Fracture toughness K_{1C} as function of strength¹³

particle size. The latter is much coarser in bainite than in martensite¹¹ (Table 2).

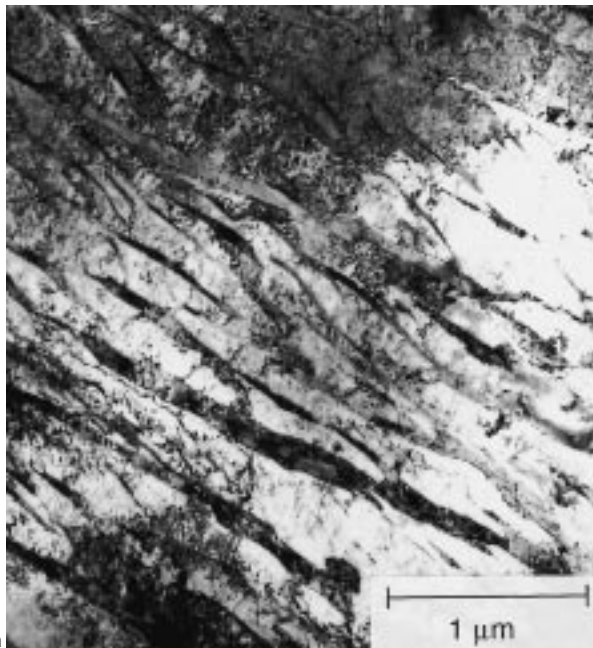
The reason for the coarser cementite in bainite is its mechanism of transformation (Fig. 6). Growth is initially diffusionless. For upper bainite the excess carbon is then rapidly partitioned into the austenite from which it precipitates as coarse cementite during the progress of the transformation. For lower bainite, the partitioning of carbon is somewhat slower because of the lower temperature so that there is an opportunity to precipitate some fine carbides within the ferrite. There is nevertheless some precipitation of cementite from carbon enriched austenite. For martensite, the carbon remains within the supersaturated plate until a tempering heat treatment can be given to precipitate fine carbides.

Better bainite

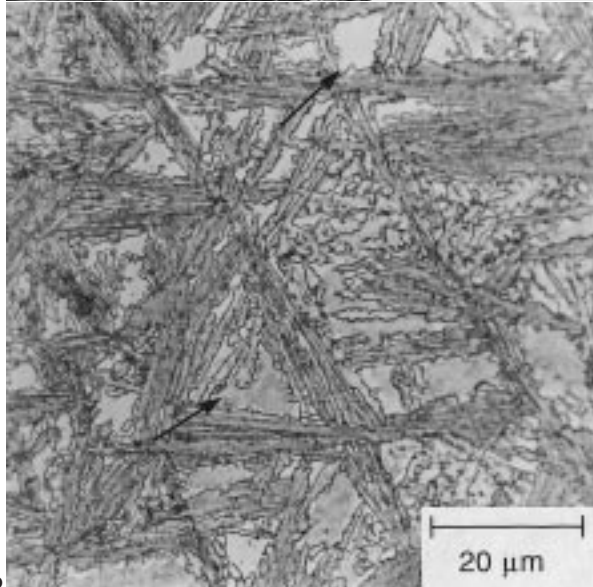
Because of the difference in the mechanism of transformation, bainitic steels have always been second best when compared with tempered martensite. The lack of toughness can in principle be eliminated by using steels with a high silicon concentration (e.g. 1.5 wt-%). Silicon has a negligible solubility in cementite and hence greatly retards its precipitation.



6 Stages in development of bainitic microstructure



a

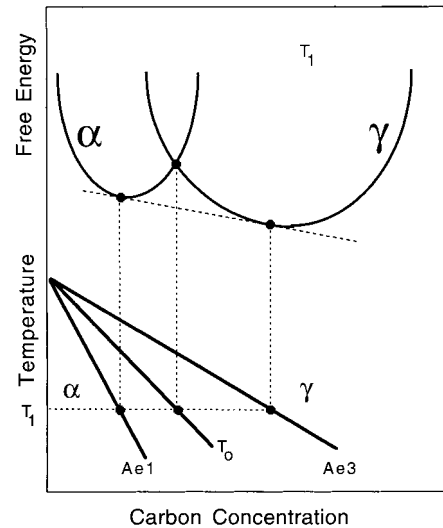


b

7 **a** transmission electron micrograph of mixture of bainitic ferrite and stable austenite; **b** optical micrograph of upper bainite in Fe-0.43C-3Mn-2.02Si steel showing blocks of retained austenite between sheaves of bainite

The transformation stops before the final stage illustrated in Fig. 6 is reached, leaving at the isothermal transformation temperature, plates of bainitic ferrite separated by films of carbon enriched austenite (Fig. 7a). There are no cementite particles to nucleate cleavage cracks or voids; the bainitic ferrite has a low concentration of dissolved carbon; strengthening and toughening is achieved by the very fine ferrite plates (a natural consequence of the transformation mechanism); there are intimately mixed ductile films of austenite to blunt any cracks and perhaps to toughen via a TRIP (transformation induced plasticity) effect; the austenite also impedes penetration of the steel by hydrogen. Evidently, a dream microstructure.

Unfortunately, this seemingly ideal microstructure does not live up to expectations. There are, in addition to the films of austenite, some large 'blocky' regions of austenite in the microstructure (Fig. 7b). The blocks are relatively unstable and transform into high carbon, untempered, brittle martensite under the influence of stress. These large



8 Schematic illustration of origin of T_0 construction on Fe-C phase diagram: austenite with carbon concentration to left of T_0 boundary can in principle transform without any diffusion; diffusionless transformation is thermodynamically impossible if carbon concentration of austenite exceeds T_0 curve; strain energy would have effect of shifting curve to lower carbon concentration, T'_0 curve

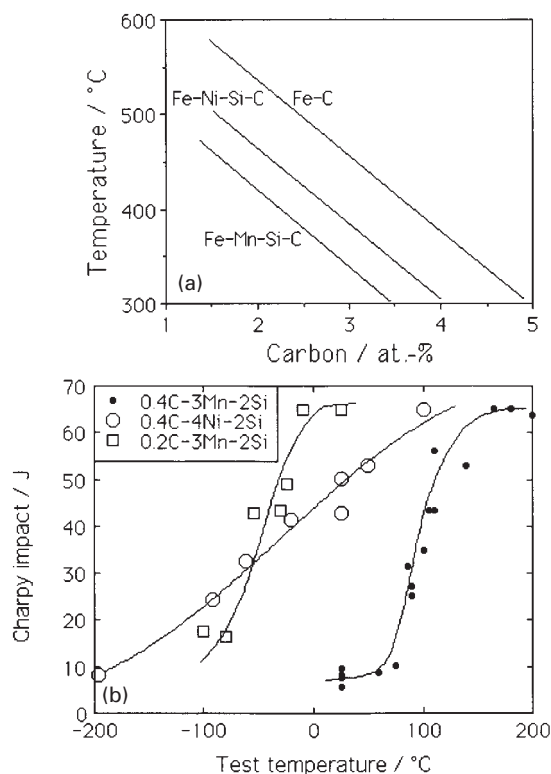
'inclusions' render the steel brittle. They are a direct consequence of the mechanism of transformation. It was noted above that bainite grows without diffusion (although the excess carbon is then redistributed). The transformation therefore becomes thermodynamically impossible once the austenite composition reaches the T'_0 curve of the phase diagram (Fig. 8). At this point, austenite and supersaturated bainitic ferrite of the same chemical composition have the same free energy. If, on the other hand, the bainite formed with its equilibrium composition, then the transformation could continue until the austenite achieves its equilibrium composition given by the usual Ae_3 curve of the phase diagram, and the blocky regions of high carbon austenite would be consumed, giving a tough steel.

The fact that bainite growth is without diffusion causes large regions of austenite to remain untransformed, no matter how long the sample is held at the transformation temperature. The blocky regions of austenite can be eliminated by promoting further transformation to bainite, either by displacing the T'_0 curve to larger carbon concentrations, or by reducing the average carbon concentration. The former can be accomplished by modifying the substitutional solute content of the steel (i.e. the phase stabilities).

Figure 9b shows the impact transition curves of three steels, the first (Fe-0.4C-3Mn-2Si) has large quantities of blocky austenite (Fig. 7b) and very poor impact toughness at room temperature. The nickel containing steel has a T'_0 curve which is at larger carbon concentrations (Fig. 9a); the Fe-0.2C-3Mn-2Si steel has half the carbon concentration of the former steel. Both these new steels have much better impact properties because the modifications allow more bainitic ferrite to form at the expense of blocky austenite.^{12,13} The better toughness is achieved without any sacrifice of strength.

Exploitation of transformation mechanism

It was demonstrated above that a strong and tough bainitic steel can be designed using the T'_0 curve. This has led to the development of novel ultrahigh strength steels with



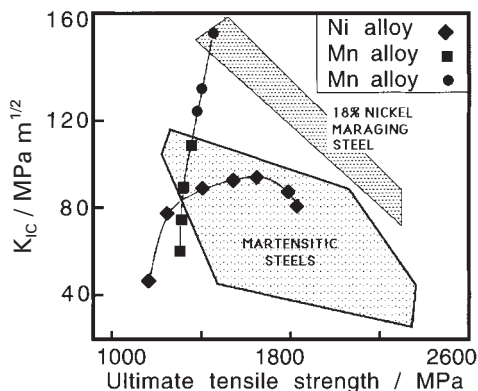
9 a calculated T_0 curves for Fe-C, Fe-Mn-Si-C, and Fe-Ni-Si-C steels; b experimentally determined impact transition curves showing how toughness improves as amount of blocky austenite is reduced; chemical compositions stated are approximate¹²⁻¹⁴

strength and toughness combinations which match or exceed more expensive alloys (Fig. 10).¹²⁻¹⁸

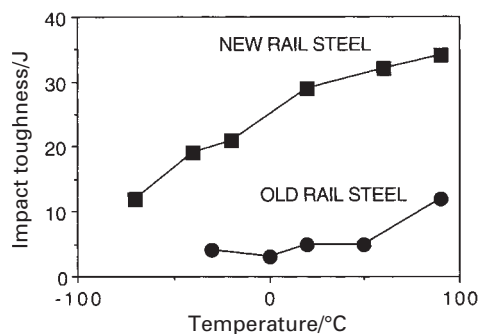
A recent application has been in rail steels which are tough and also exceptionally resistant to fatigue and wear.¹⁸ The microstructure of conventional rails is based on a mixture of cementite and ferrite in the form of pearlite. The cementite is hard and therefore provides wear resistance, but it is also brittle. The new bainitic rail steel is completely free of carbides; it has a much higher toughness but is harder due to the fine grain size and residues of martensite and retained austenite (Fig. 11).

Mechanism and strength

The equilibrium shape of ferrite in austenite is that of an equiaxed idiomorph. Many varieties of ferrite nevertheless



10 New, cheap bainitic steels (points) which match properties of expensive alloys¹⁵⁻¹⁷



11 Toughness of new and conventional rail steels

grow in the form of plates. These all grow by the displacive mechanism described above, so that their growth causes the shape of the transformed region to change, the change being an invariant plane strain (IPS) with a large shear (Table 3). This is not the case when the ferrite grows in any other shape. A small aspect ratio (plate thickness/plate length) leads to a better accommodation of the plate and hence to a minimisation of the elastic strains in the austenite.

Processes of plastic deformation absorb a lot more energy than when cleavage occurs. Therefore, most mechanisms of strengthening lead to a decrease in toughness. The exception is grain size strengthening, where a refinement of the microstructure simultaneously improves the strength and toughness. In this respect, a plate shape is better than an equiaxed grain structure. The mean free slip distance through a plate is only about twice its thickness,²⁴ which for bainite is typically far less than a micrometre in size. The accelerated cooled thermomechanically processed steels with bainitic microstructures rely on this. Quantitative details about the strengths of bainite and martensite can be found in Refs. 8 and 14.

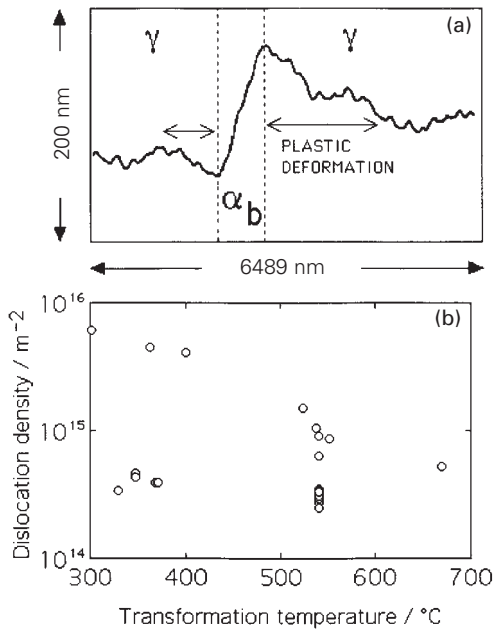
Further plate refinement

Martensite and bainite plates sometimes stop growing before they impinge with a hard obstacle such as a grain boundary or another plate. Such tiny plates which are prematurely halted are called 'subunits' (Fig. 6) because they grow in clusters called sheaves. Within each sheaf the subunits are parallel and of identical crystallographic orientation and habit plane. The subunits are usually separated from each other either by carbide particles or residual austenite.²⁵⁻²⁷

When transformation occurs at high temperatures, the shape deformation causes the relatively weak austenite to deform plastically. Figure 12 illustrates the irreversible deformation caused in the adjacent austenite by the transformation. The resulting forest of dislocations blocks the progress of the glissile transformation interface, which explains why the subunit stops growing even though it may not have encountered an austenite grain surface. In fact, the size can be decreased further by causing the bainite

Table 3 Approximate values of shear s and dilatational δ strains accompanying formation of transformation products in steels

Transformation product	s	δ	Morphology	Ref.
Widmanstätten ferrite	0.36	0.03	Thin plates	19
Bainite	0.22	0.03	Thin plates	20, 21
Martensite	0.24	0.03	Thin plates	22, 23
Allotriomorphic ferrite	0	0.03	Irregular	
Idiomorphic ferrite	0	0.03	Equiaxed	



12 a high resolution atomic force microscope plot of displacements caused by formation of single subunit of bainite: surface was flat before transformation (note plastic deformation caused in adjacent austenite);²¹ b dislocation density of martensite, bainite, and Widmanstätten ferrite as function of transformation temperature

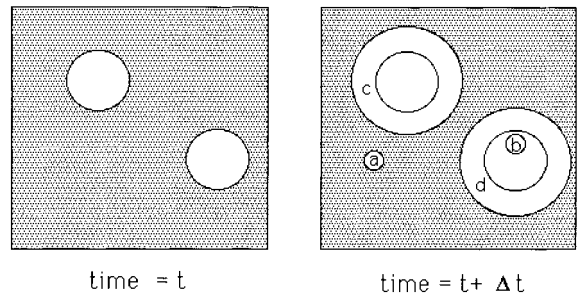
to grow in plastically deformed austenite;²⁸ there is evidence to suggest that thermomechanically processed bainitic steels benefit from this *mechanical stabilisation*.

The plastic relaxation of the shape change causes an increase in the dislocation density of bainitic ferrite since any motion of the interface into the deformed austenite will cause the defect structure to be inherited. Thus, although there is considerable scatter in published data, the dislocation density generally decreases as the transformation temperature is increased (Fig. 12b).

Simultaneous transformations

The steels discussed above are for high strength applications and for service conditions where the maximum temperature is never far from ambient. The most modern creep resistant steels for elevated temperature service are bainitic or martensitic but in a secondary hardened condition. The evolution of the secondary hardened microstructure is very complex, involving the precipitation and dissolution of many metastable alloy carbides. Avrami theory can be used to estimate the time-temperature-transformation diagram for the carbide precipitation reactions. This is introduced in terms of conventional Avrami theory which deals with isolated reactions; an exciting recent development which permits the treatment of more than one reaction occurring at the same time is then introduced.

A model for a single precipitation reaction begins with the calculation of the nucleation and growth rates using classical theory, but an estimation of the volume fraction requires impingement between particles to be taken into account. This is generally done using the extended volume concept of Johnson *et al.*,²⁹ as illustrated in Fig. 13. Suppose that two particles exist at time *t*; a small interval Δt later, new regions marked a, b, c, and d are formed, assuming that they are able to grow unrestricted in extended space, whether or not the region into which they grow is already transformed. However, only those components of a, b, c,



13 Illustration of concept of extended volume: two precipitate particles have nucleated together and grown to finite size in time *t*; new regions c and d are formed as original particles grow, but a and b are new particles, of which b has formed in a region which is already transformed

and d which lie in previously untransformed matrix can contribute to a change in the real volume of the product phase (identified by the subscript 1)

$$dV_1 = [1 - (V_1/V)] dV_1^e \dots \dots \dots (4)$$

where it is assumed that the microstructure develops randomly. The superscript *e* refers to extended volume, *V*₁ is the volume of 1, and *V* is the total volume. Multiplying the change in extended volume by the probability of finding untransformed regions has the effect of excluding regions such as b, which clearly can not contribute to the real change in volume of the product. This equation can easily be integrated to obtain the real volume fraction as

$$V_1/V = 1 - \exp(-V_1^e/V) \dots \dots \dots (5)$$

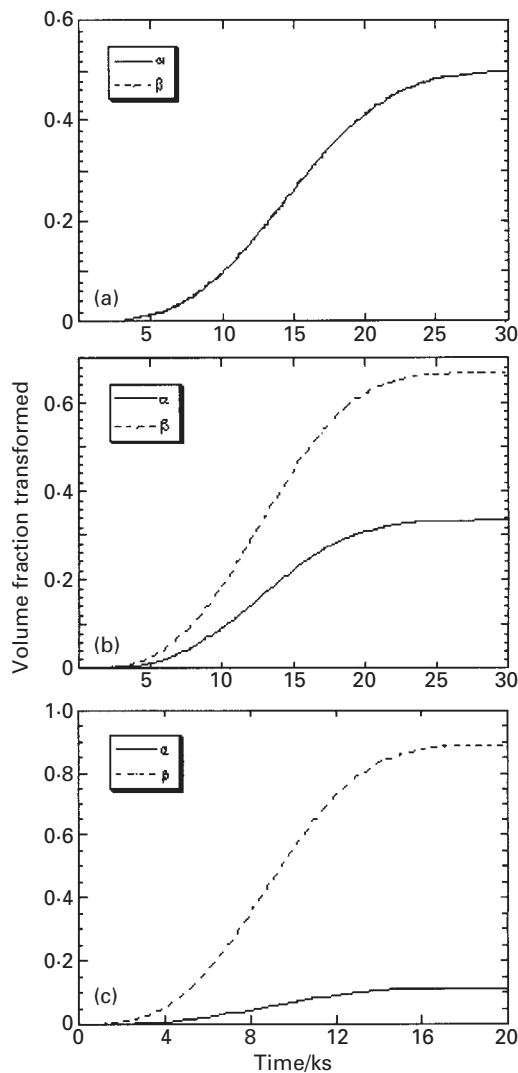
In practice, there are many cases where several transformations occur together. The different reactions interfere with each other in a way which is seminal to the development of power plant microstructures. Therefore, considerable effort has recently been devoted to the development of an Avrami model for simultaneous reactions.^{30,31} A simple explanation for two precipitates (1 and 2) is that the above equation becomes a set of two equations

$$\begin{aligned} dV_1 &= \{1 - [(V_1 + V_2)/V]\} dV_1^e \} \\ dV_2 &= \{1 - [(V_1 + V_2)/V]\} dV_2^e \} \dots \dots \dots (6) \end{aligned}$$

which in general must be solved numerically although an analytical solution has been proposed for the case where the ratio of the volume fractions of the two phases is constant.^{30,31} The method can in principle be extended to incorporate an indefinite number of reactions happening together.

Some example calculations are presented in Fig. 14. When the nucleation and growth rates of α and β are set to be exactly identical, their curves for volume fraction versus time are exactly superimposed and each phase eventually achieves a fraction of 0.5 (Fig. 14a). When the nucleation rate of β is set to equal twice that of α , then for identical growth rates, the terminal fraction of β is, as expected, twice that of α (Fig. 14b). The case where the growth rate of β is set to be twice that of α (with identical nucleation rates) is illustrated in Fig. 14c.

A more complicated description for a power plant steel is illustrated in Fig. 15. The cementite forms first, then begins to dissolve with the precipitation of both M_2C and $M_{23}C_6$. It is interesting to compare this alloy (a 10Cr-1Mo steel) with the Baker and Nutting³² (2.25Cr-1Mo) steel. Precipitation of $M_{23}C_6$ is very slow indeed in the Baker and Nutting steel, because the relatively rapid precipitation of M_2C stifles that of $M_{23}C_6$. Precipitation of M_2C is slower in the 10Cr-1Mo steel because the cementite enriches rapidly, thereby reducing the driving force for the



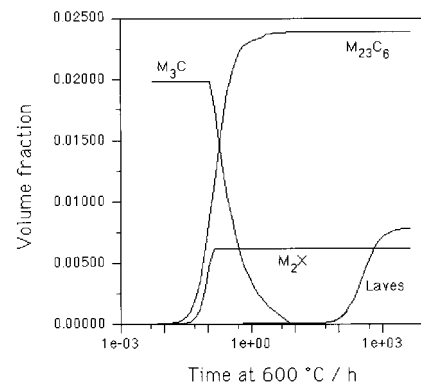
a when two phase have identical nucleation and growth rates; b identical growth rates but with β having twice the nucleation rate of α ; c identical nucleation rates but with β particles growing at twice rate of α particles

14 Illustration of kinetics of two reactions occurring simultaneously

precipitation of the M_2C . These phenomena could not have been predicted without the treatment of simultaneous kinetics, and provide a method for delaying the precipitation of $M_{23}C_6$, believed by some to be important in order to retard the subsequent formation of Laves phases.

The calculations rely on a number of assumptions which include the following:

- (i) the model allows for the simultaneous precipitation of M_2X , $M_{23}C_6$, and Laves phase. The M_3C is assumed to nucleate instantaneously with the para-equilibrium composition. Subsequent enrichment of M_3C as it approaches its equilibrium composition is accounted for
- (ii) all the phases, except M_3C , form close to their equilibrium composition. The driving forces and compositions of the precipitating phases are calculated using MTDATA, a phase diagram and thermodynamic database package
- (iii) the interaction between the precipitating phases is accounted for by considering the change in the average solute level in the matrix as each phase forms
- (iv) the model does not require prior knowledge of the precipitation sequence
- (v) dissolution of non-equilibrium phases is incorporated



15 Calculated evolution³⁰ of phase fractions in a 9Cr-Mo-V-W steel (NF616) during tempering at 600°C

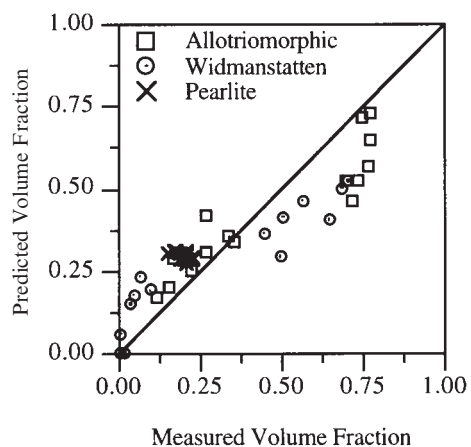
- (vi) a single set of fitting parameters for the nucleation equations (site densities and surface energies) has been found which is applicable to a wide range of power plant steels.

Microstructure maps for structural steels

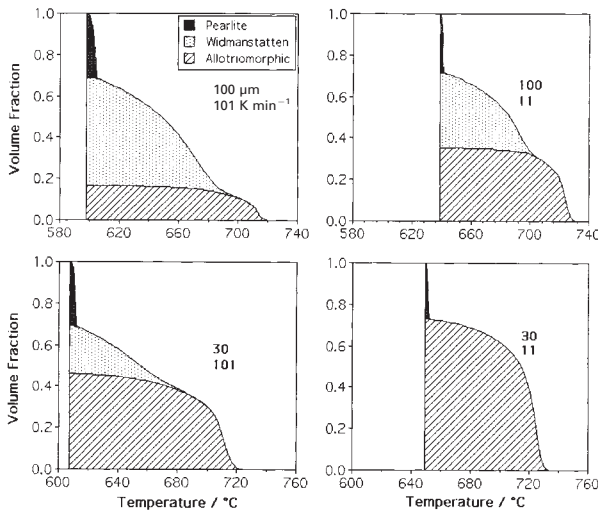
The methods described for creep resistant steels can be applied more generally. The figures that follow show calculations which illustrate how the simultaneous transformations model can be used to study the evolution of microstructure as the samples of structural steels cool.³¹ The calculations are for the steel composition Fe-0.18C-0.18Si-1.15Mn-0.015P-0.030S-0.026Al-0.09Cu-0.0073N (<0.005%Nb, <0.003%V). The phases involved in this case are allotriomorphic ferrite, Widmanstätten ferrite, and pearlite.

The reasonable overall level of agreement between experiment and theory is illustrated in Fig. 16, for all of the data from Ref. 33. In all cases where the allotriomorphic ferrite content is underestimated, the Widmanstätten ferrite content is overestimated. This is expected both because the composition of the austenite changes when allotriomorphic ferrite forms and because its formation changes the amount of austenite that is free to transform to Widmanstätten ferrite.

All the generally recognised trends are reproduced. The amount of Widmanstätten ferrite clearly increases with the austenite grain size, and with the cooling rate within the range considered. Bodnar and Hansen³³ suggested also that the effect of cooling rate on the amount of



16 Comparison of calculated volume fraction with experimental data reported by Bodnar and Hansen³³



17 Calculated³¹ evolution of microstructures in samples with given austenite grain sizes and cooling rates

Widmanstätten ferrite was smaller than that of the austenite grain size (for the values considered). This is also evident in Fig. 17.

Conclusions

It has been demonstrated for a few cases that both thermodynamic and kinetic theory can be used effectively in the design of steels. It is interesting that the complexity of steels is driving the development of phase transformation theory; for example, in the adaptation of the classical Avrami model for isolated reactions to one capable of handling many reactions at the same time.

It has not been possible in this paper to comment on other exciting developments which are of equal importance in research and development. For example, it is frequently frustrating to be able to model the microstructure with considerable accuracy, but then become hindered by the lack of microstructure–property relationships. This is particularly difficult for complex properties such as fatigue and toughness. The application of neural network analysis to such problems is a growing area in metallurgy and has already led to commercial products. But that is another story.

References

1. H. K. D. H. BHADESHIA: *Prog. Mater. Sci.*, 1985, **29**, 321–286.
2. A. CHRISTOU and N. BROWN: *J. Appl. Phys.*, 1971, **42**, 4160–4170.

3. P. M. GILES, M. H. LONGENBACH, and A. R. MARDER: *J. Appl. Phys.*, 1971, **42**, 4290–4295.
4. J. W. CHRISTIAN: 'Theory of transformations in metals and alloys'; 1965, Oxford, Pergamon Press.
5. M. S. WECHSLER, D. S. LIEBERMAN, and T. A. READ: *Trans. AIME*, 1953, **197**, 1503–1515.
6. J. S. BOWLES and J. K. MACKENZIE: *Acta Metall.*, 1954, **2**, 129–137.
7. C. M. WAYMAN and H. K. D. H. BHADESHIA: in 'Physical metallurgy', 3rd edn, (ed. R. W. Cahn and P. Haasen), 1508–1554; 1997, Amsterdam, North Holland.
8. H. K. D. H. BHADESHIA: 'Bainite in steels'; 1992, London, The Institute of Materials.
9. D. A. CURRY and J. F. KNOTT: *Met. Sci.*, 1978, **12**, 511–514.
10. J. F. KNOTT: in 'Micromechanisms of fracture and their structural significance, proceedings of the second Griffith conference', 3–14; 1995, London, The Institute of Materials.
11. P. BOWEN, S. G. DRUCE, and J. F. KNOTT: *Acta Metall.*, 1986, **34**, 1121–1131.
12. H. K. D. H. BHADESHIA and D. V. EDMONDS: *Met. Sci.*, 1983, **17**, 411–419.
13. H. K. D. H. BHADESHIA and D. V. EDMONDS: *Met. Sci.*, 1983, **17**, 420–425.
14. R. W. K. HONEYCOMBE and H. K. D. H. BHADESHIA: 'Steels', 302–318; 1995, London, Edward Arnold.
15. V. T. T. MIIHKINEN and D. V. EDMONDS: *Mater. Sci. Technol.*, 1987, **3**, 422–431.
16. V. T. T. MIIHKINEN and D. V. EDMONDS: *Mater. Sci. Technol.*, 1987, **3**, 432–440.
17. V. T. T. MIIHKINEN and D. V. EDMONDS: *Mater. Sci. Technol.*, 1987, **3**, 441–449.
18. H. K. D. H. BHADESHIA: in 'Future developments of metals and ceramics', (ed. J. A. Charles *et al.*), 25–74; 1992, London, The Institute of Materials.
19. J. D. WATSON and P. G. McDUGALL: *Acta Metall.*, 1973, **21**, 961–973.
20. B. J. P. SANDVIK: *Metall. Trans. A*, 1982, **13A**, 777–800.
21. E. SWALLOW and H. K. D. H. BHADESHIA: *Mater. Sci. Technol.*, 1996, **12**, 121–125.
22. C. M. WAYMAN: 'Introduction to the crystallography of martensite'; 1964, New York, Macmillan.
23. D. P. DUNNE and C. M. WAYMAN: *Metall. Trans.*, 1971, **2**, 2327–2341.
24. J. DAIGNE, M. GUTTMAN, and J. P. NAYLOR: *Mater. Sci. Eng.*, 1982, **56**, 1–10.
25. R. F. HEHEMANN: 'Phase transformations', 397–432; 1970, Metals Park, OH, ASM.
26. H. K. D. H. BHADESHIA and D. V. EDMONDS: *Acta Metall.*, 1980, **28**, 1265–1273.
27. S. KAJIWARA: *Philos. Mag. A*, 1981, **43**, 1483–1503.
28. P. SHIPWAY and H. K. D. H. BHADESHIA: *Mater. Sci. Technol.*, 1995, **11**, 1116–1128.
29. J. W. CHRISTIAN: 'Theory of transformations in metals and alloys', 2nd edn, Part 1; 1975, Oxford, Pergamon Press.
30. J. D. ROBSON and H. K. D. H. BHADESHIA: *Mater. Sci. Technol.*, 1997, **13**, 631–639.
31. S. J. JONES and H. K. D. H. BHADESHIA: *Acta Mater.*, 1997, **45**, 2911–2920.
32. R. G. BAKER and J. NUTTING: *J. Iron Steel Inst.*, 1959, **192**, 257–268.
33. R. L. BODNAR and S. S. HANSEN: *Metall. Mater. Trans. A*, 1994, **25A**, 763–773.